Vector Control of Asynchronous Generators in No-Load Mode

Olimjon Toirov[1,a)], Mirzokhid Taniev[1], Zuvur Toirov[2], Jasur Karimov[1], Dilruh Omonboev[1], Shakhlo Khodjaeva[1]

[1]*Tashkent State Technical University named after Islam Karimov, Tashkent, Uzbekistan*
[2]*Bukhara State Technical university, Bukhara, Uzbekistan*

[a] *Corresponding author: olimjontoirov@gmail.com*

Abstract. This article presents the parallel operation of a doubly fed induction generator (DFIG) with an electrical grid under varying wind and water flow velocities, as well as vector control methods. Attention is paid to the stability of the electrical system and the safety of generators when connected to the grid. Assuming that the stator current in no-load mode is zero, i_{ds}=i_{qs}=0, the voltage equation and the current relationship equation for two-pole asynchronous generators are presented. Mathematical models of two-pole asynchronous generators in no-load mode are presented. The equation shows the relationship between the rotor axis current component and the target stator load voltage Us. Formulas for calculating the reactive power and rotor winding losses of a DFIG operating in no-load mode are presented. A block diagram of the control strategy and vector control for the DFIG motion in no-load mode is presented. A PI controller is calculated for a first-order system. As an example, the speed control of a grid-connected DFIG is considered, and an internal current controller and an external speed controller are developed. In both cases, PI controllers are used, the parameters of which are developed using EMF theory and the pole placement method, respectively. A block diagram of the closed-loop control system for speed control is presented.

INTRODUCTION

In order to parallel the generators to the power supply system, it is usually required that the generators are in normal operation. In this case, the connection to the grid directly affects the stability of the power system, as well as the safety of the generators[1-5].

The process of connecting induction generators to the grid, which are powered by two times the constant frequency with variable wind and water parameters, is significantly different from that of synchronous and conventional asynchronous generators driven by DC. Synchronous or conventional asynchronous generators driven by DC have a rigid connection to the power system. For synchronous generators, the generator output frequency is completely dependent on the speed of the prime mover. Before connecting to the grid, the generator must be strictly synchronized. After the generator is connected to the grid, its speed must be kept constant. Otherwise, the frequency at the generator output will change[6]. On the other hand, asynchronous generators have lower requirements for the accuracy of speed adjustment. There is no oscillation or desynchronization phenomenon after grid connection. Doubly-fed induction generators use a grid connection method similar to ordinary synchronous generators, that is, the generator that has already been started is connected to the grid after the grid connection conditions are met. DFIG s, due to their adaptive connection to the power system, have separated the stator voltage frequency and rotor speed, which ensures grid connection under variable speed conditions[7]. Therefore, before grid connection, the excitation power source on the rotor side of the DFIG adjusts the excitation current according to the grid voltage and generator speed, and thus adjusts the amplitude, frequency and phase of the generator output voltage to adapt to the grid no-load operation of the DFIG.

EXPERIMENTAL RESEARCH

In the operating area diagram of the wind turbine generator set, OA and AB represent the startup phase. In segment OA, the doubly-fed induction generator operates under no-load conditions and is controlled for grid connection; in segment AB, after successful grid connection, the doubly-fed generator control strategy switches from grid connection control to normal power generation control mode[8-12]. The control objective of the doubly-fed induction generator operating under no-load conditions is the same as that of independent operation, which is to control the stator voltage.

The differences are:

1. The doubly-fed induction generator operating under no-load conditions outputs a grid-connected voltage on the stator side that meets the grid connection conditions, i.e., outputs a stator voltage with the same frequency, amplitude, and phase as the grid voltage. In independent operation, the stator voltage does not need to track a specific voltage[13];

2. During no-load operation, the stator current of the doubly-fed induction generator is 0, which simplifies the generator model. Under no-load operation, the stator current is zero, $i_{ds}=i_{qs}=0$, under this condition, the voltage equation and flux linkage equation of the doubly-fed induction generator simplify to[14-16]:

$$\begin{aligned} \psi_{ds} &= L_0 i_{dr} \\ \psi_{qs} &= L_0 i_{qr} \\ \psi_{dr} &= L_r i_{dr} \\ \psi_{qr} &= L_r i_{qr} \end{aligned} \tag{1}$$

$$\begin{aligned} u_{ds} &= p\psi_{ds} - \omega_1 \psi_{qs} \\ u_{qs} &= p\psi_{qs} - \omega_1 \psi_{ds} \\ u_{dr} &= R_r i_{dr} + p\psi_{dr} - \omega_2 \psi_{qr} \\ u_{qr} &= R_r i_{qr} + p\psi_{qr} - \omega_2 \psi_{dr} \end{aligned} \tag{2}$$

Still oriented the stator flux linkage on the *d*-axis, $\psi_{qs}= 0$ and $\psi_{ds}= \psi_s$, $\psi_{qs}= 0$ according to equation (1), to achieve stator flux linkage coinciding with the *d*-axis, control i_{qr} to be 0, then the command value of the rotor *q*-axis current component i_{qr}^*

$$i_{qr}^* = 0 \tag{3}$$

From ds s

$\psi_{ds}=\psi_s$, according to equation (1), we get

$$i_{dr} = \psi_s / L_0 = i_{ms} = U_s / \omega_1 L_0 \tag{4}$$

Equation (4) shows that during no-load operation, the generator's excitation current is entirely provided by the rotor *d*-axis current component[17-20].

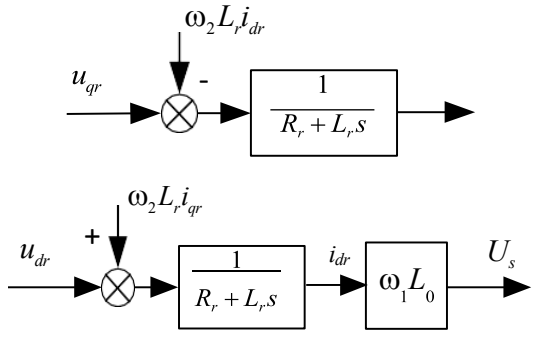

FIGURE 1. Mathematical Model of Doubly Fed Induction Generator in No-Load Operation

Therefore, the voltage equation in Equation (2) can be simplified to.

$$u_{ds} = L_0 p i_{dr}$$
$$u_{qs} = \omega_1 L_0 p i_{dr} = \omega_1 \psi_s$$
$$u_{dr} = (R_r + L_r p) i_{dr} - \omega_2 L_r i_{qr} \tag{5}$$

From the stator voltage part of equation (5), it can be seen that when the doubly fed induction generator in no-load operation reaches steady state, u_{ds} =0, u_{qs}=$\omega_1 \Psi_s$ = U_s, realizing the orientation of the stator side no-load voltage on the q-axis.

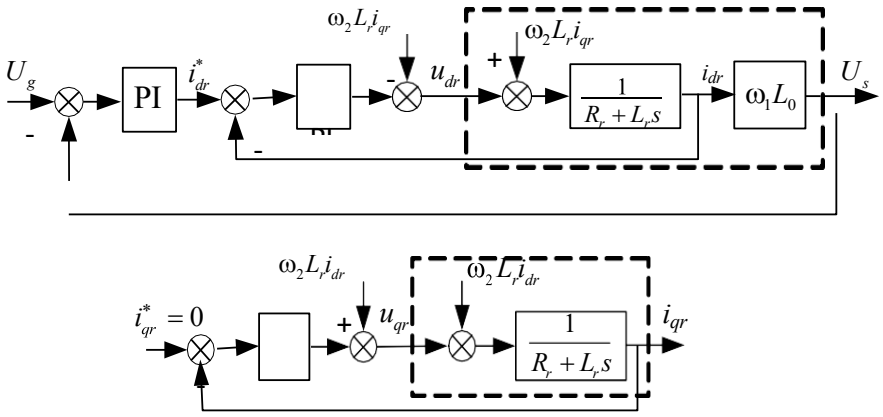

FIGURE 2. Control block diagram of doubly-fed induction generator under no-load operation

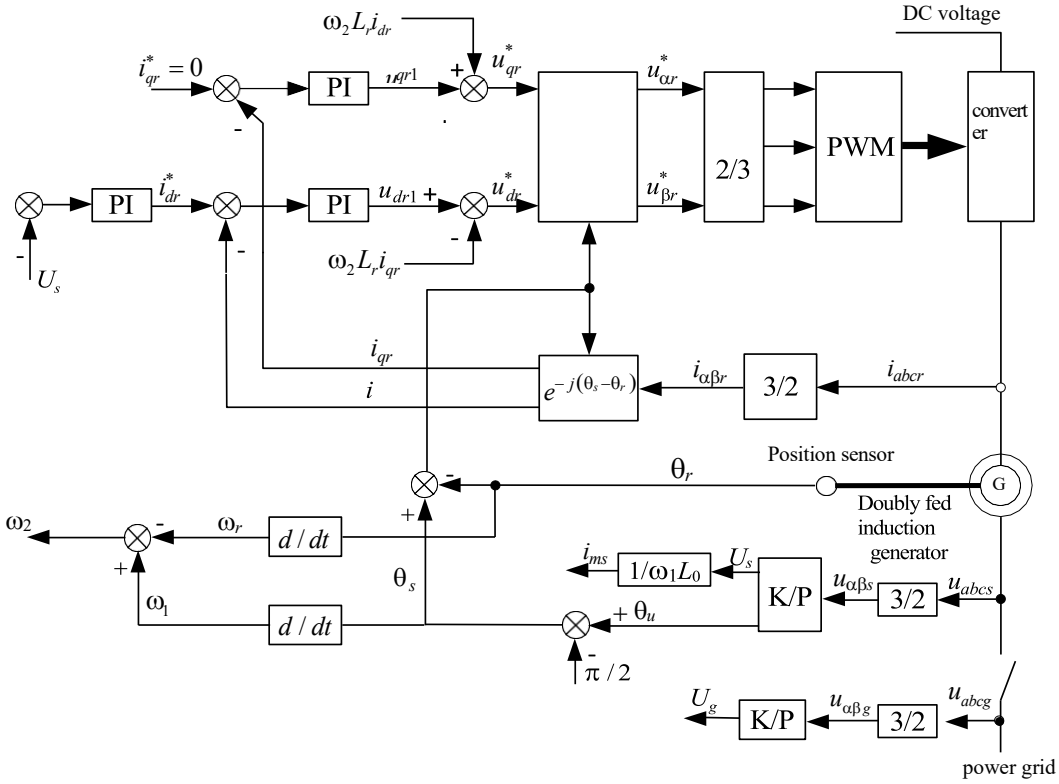

FIGURE 3. Block diagram of excitation vector control strategy for doubly-fed induction generator under no-load operation

The relationship between the rotor d-axis current component and the control target stator side no-load voltage Us is shown in equation (4) [21-22]. Therefore, the mathematical model of the doubly fed induction generator in no-load operation is shown in Figure 1.

The doubly-fed induction generator (DFIG) operating under no-load conditions provides excitation reactive power and a small amount of rotor winding losses. The control objective is the stator-side no-load voltage. To track the grid voltage, the grid voltage vector magnitude U_g is used as the control objective value for the outer voltage loop. The excitation control block diagram of the rotor-side converter during no-load operation is shown in Figure 2. Figure 3 shows the excitation vector control strategy block diagram of the DFIG during no-load operation[23-24].

This section takes the speed mode control of a grid-connected doubly-fed induction generator as an example and designs an inner current controller and an outer speed controller. Both the inner current controller and the outer speed controller adopt PI controllers, and the parameters of the PI controllers are designed using IMC theory and pole placement, respectively[25-29].

The current closed-loop control system based on internal model control (IMC) theory exhibits good tracking performance and anti-interference capability. For a first-order system, the controller is a PI controller.

Baseline model of the controlled object

$$\tilde{P}(s) = \frac{1}{R_r + \sigma L_r s} \tag{6}$$

Internal mold controller

$$Q(s) = \tilde{P}^{-1}(s) \cdot F(s) \tag{7}$$

Where $F(s)$ is a first-order filter, $F(s) = 1/(\tau s + 1)$, and τ is the filter parameter. The transfer function of the PI controller is expressed as

$$C(s) = \frac{Q(s)}{1 - Q(s)\tilde{P}(s)} = \frac{\tilde{P}^{-1}(s)F(s)}{1 - F(s)} = \frac{\tilde{P}^{-1}(s)}{\frac{1}{F(s)} - 1} = \frac{R_r + \sigma L_r s}{\tau s} \tag{8}$$

Again

$$C(s) = K_{pc} + \frac{K_{ic}}{s} \tag{9}$$

Comparing equations (8) and (9), we obtain the proportional gain and integral gain of the current inner-loop PI controller.

$$K_{pc} = \frac{\sigma L_r}{\tau}$$
$$K_{ic} = \frac{R_r}{\tau} \tag{10}$$

As can be seen from equation (10), a reasonable PI parameter can be obtained by adjusting only one filter parameter, and the relationship between the filter parameter and the dynamic steady-state performance and robust stability performance of the system is clear.

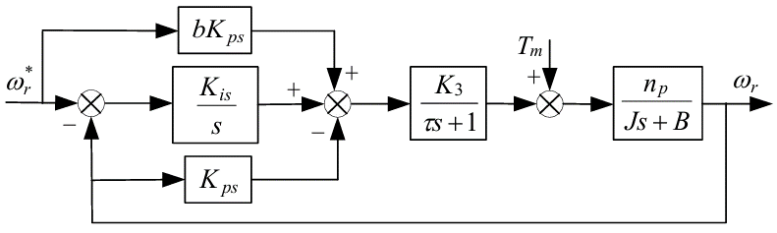

FIGURE 4. Block diagram of the closed-loop control system for speed mode control

The speed outer loop controller adopts a PI controller with parameter *b* introduced. The inner loop command value of the current output by the speed outer loop controller is expressed as follows:

$$i_{qr}^{*} = K_{pc}(b\omega_r^{*} - \omega_r) + K_{is}\int(\omega_r^{*} - \omega_r)dt \tag{11}$$

Where K_{ps} and K_{is} are the proportional gain and integral gain of the speed outer loop controller, respectively.

Figure 4 is a block diagram of the closed-loop control system under speed mode control. The current inner loop has a very fast response speed, equivalent to a small inertial element 1/(sτ+1).

RESEARCH RESULTS

Based on the closed-loop control system block diagram, consider the transfer function relationship of the closed-loop output speed ω_r* of the doubly-fed generator under the simultaneous action of the reference input speed signal ω_r and the input mechanical torque T_m:

$$\omega_r(s) = G_{i0}(s)\omega_r^{*}(s) + G_{d0}(s)T_m(s) \tag{12}$$

G_{io}(s) controls the input-to-output transfer function:

$$G_{i0}(s) = \frac{K_4(bK_{ps}s + K_{is})}{\tau\tau_1 s^3 + (\tau+\tau_1)s^2 + (K_{ps}+K_4+1)s + K_{is}K_4} \tag{13}$$

G_{do}(s) is the transfer function from mechanical torque disturbance to output:

$$\begin{aligned} G_{d0}(s) &= \frac{K_4(bK_{ps}s + K_{is}G_{i0}(s))}{\tau\tau_1 s^3 + (\tau+\tau_1)s^2 + (K_{ps}+K_4+1)s + K_{is}K_4}(s) = \\ &= \frac{n_p(\tau s+1)s/B}{\tau\tau_1 s^3 + (\tau+\tau_1)s^2 + (K_{ps}+K_4+1)s + K_{is}K_4} \end{aligned} \tag{14}$$

In equations (13) and (14), $K_4 = L_0 n_p^2 U_s / L_s \omega_1 B$, $\tau_1 = B/J$. Characteristic equation of the closed-loop system:

$$D(s) = \tau\tau_1 s^3 + (\tau+\tau_1)s^2 + (K_{ps}+K+1)s + K_{is}K_4 \tag{15}$$

The closed-loop control system is a third-order system. The controller PI parameters are tuned using the state pole placement method.

Optimizing the closed-loop poles can effectively improve the system's dynamic performance. For higher-order systems, dynamic performance indicators are primarily determined by the dominant closed-loop poles. System dominant closed-loop poles:

$$s_{1,2} = -\zeta\omega_r \pm j\omega_r\sqrt{1-\zeta_r^2} \tag{16}$$

Simultaneously, the closed-loop non-dominant pole is selected:

$$s_3 = -n\zeta_r\omega_r \tag{17}$$

Where ζ_r and ω_r are the desired damping ratio and natural oscillation frequency, respectively.

The value of *n* determines the location of the non-dominant closed-loop poles in the complex plane. The larger *n* is, the closer the response characteristics of the third-order system determined by the three poles (s_3, s_2, and s_1) are to those of the second-order system determined by the dominant pole. Typically, *n* is taken as *n* = 5−10.

The characteristic equation of the third-order system determined by 1s, 2s, and 3s is:

$$\begin{aligned} D_s(s) &= (s-s_1)(s-s_2)(s-s_3) = (s^2 + 2\zeta_r\omega_r s - \omega_r{}^2)(s + n\zeta_r\omega_r - \omega_r) = \\ &= s^3 + (n+2)\zeta_r\omega_r s^2 + \omega_r{}^2(2n\zeta^2{}_r + 1)s + n\zeta_r\omega_r^3 \end{aligned} \tag{18}$$

Comparing equations (15) and (18), the PI coefficient is obtained as follows:

$$\begin{aligned} K_{ps} &= \left[\omega_r^2\tau\tau_1(2n\zeta_r^2+1) - 1\right]/K_4 \\ K_{is} &= \tau\tau_1\omega_r^3 n\zeta_r / K_4 \end{aligned} \tag{19}$$

Wherein, n, ζ_r, ω_r, τ and τ_1 satisfy the following relationship:

$$(n+2)\zeta_r\omega_r = \frac{\tau+\tau_1}{\tau\tau_1} \tag{20}$$

Subsequent simulation studies show that although ζ_r takes a value greater than 1, the system still has overshoot due to the influence of the zero point introduced by the PI controller. Therefore, a coefficient b is introduced into the PI controller. As shown in equation (13), the b parameter allows the zero point position to be set independently. In particular, setting b to zero causes the zero point position introduced by the PI controller to tend towards negative infinity, thus eliminating its influence on the closed-loop time response.

CONCLUSION

In order to meet the power frequency condition for grid connection, the speed of the synchronous generator must be strictly synchronized. To do this, the grid connection is required when the speed is close to the synchronous speed (90% ~ 100%). In order to reduce the impact of the generator on the power system during parallel operation with the grid, both DFIGs and synchronous generators must meet the parallel connection conditions. Synchronous generators are excited by direct current. Unlike synchronous generators, DFIGs are excited by alternating current.

The current closed-loop control system based on the internal model control (IMC) theory has demonstrated good tracking performance and anti-interference ability. The controller for the first-order system is the PI controller. It can be seen from the above equation that by adjusting only one filter parameter, a reasonable PI parameter can be obtained. The relationship between the filter parameter and the dynamic steady-state operation of the system and the robust stability indicators can be seen.

A block diagram of the excitation vector control strategy during pure operation for a doubly powered induction generator is developed. A PI controller with an input speed external controller parameter is adopted. The internal command value of the output current is expressed by the external speed controller.

REFERENCES

1. Umarov, S., & Tulyaganov, M. (2024). Peculiarities of simulation of steady modes of valve converters with periodic power circuit structure. AIP Conference Proceedings. https://doi.org/10.1063/5.0218869
2. K. Allaev, J. Toshov, Modern state of the energy sector of Uzbekistan and issues of their development, E3S Web of Conferences 401, 05090 (2023). https://doi.org/10.1051/e3sconf/202340105090
3. O. Toirov, Sh. Azimov, Z. Toirov. Improving the cooling system of reactive power compensation devices used in railway power supply // AIP Conference Proceedings, 3331, 1, 050030, (2025). https://doi.org/10.1063/5.0305670
4. M. Taniev, B. Safarov, Z. Toirov. Simulation model of an asynchronous generator integrated with a power supply system at different wind speeds // AIP Conf. Proc. 3331, 060025 (2025). https://doi.org/10.1063/5.0305672
5. O. Toirov, M. Taniev, M. Hamdamov, A. Sotiboldiev, Power Losses Of Asynchronous Generators Based On Renewable Energy Sources E3S Web of Conferences, 434, 01020, (2023) https://doi.org/10.1051/e3sconf/202343401020
6. Sh. Azimov, Z. Najmitdinov, M. Sharipov, Z. Toirov. Improvement of the cooling system of reactive power compensating devices used in railway power supply // E3S Web of Conferences, 497, 01015, (2024). https://doi.org/10.1051/e3sconf/202449701015
7. D. Jumaeva, O. Toirov, B. Numonov, N. Raxmatullaeva, M. Shamuratova. Obtaining of highly energy-efficient activated carbons based on wood, // E3S Web of Conferences 410, 01018, (2023). https://doi.org/10.1051/e3sconf/202341001018
8. O. Toirov, D. Bystrov, S. Giyasov, M. Taniev, S. Urokov. Role of Reengineering in Training of Specialists // ACM International Conference Proceeding Series (2020) https://doi.org/10.1145/3386723.3387868
9. D. Jumaeva, O. Toirov, U. Raximov, O. Ergashev, A. Abdyrakhimov. Basic thermodynamic description of adsorption of polar and nonpolar molecules on AOGW, // E3S Web of Conferences 425, 04003 (2023) https://doi.org/10.1051/e3sconf/202343401020

10. O. Toirov, S. Khalikov, Sodikjon Khalikov, F. Sharopov, Studies of reliability indicators of pumping units of machine irrigation on the example of the "Namangan" pumping station, // E3S Web of Conferences 410, 05015, (2023). https://doi.org/10.1051/e3sconf/202341005015
11. O. Toirov, V. Ivanova, V. Tsypkina, D. Jumaeva, D. Abdullaeva, Improvement of the multifilament wire lager for cable production, // E3S Web of Conferences 411, 01041 (2023), https://doi.org/10.1051/e3sconf/202341101041
12. D. Bystrov, S. Giyasov, M. Taniev, S. Urokov. NISS2020: Proceedings of the 3rd International Conference on Networking, Information Systems & Security, 49, p. 1–4 (2020), https://doi.org/10.1145/3386723.3387868.
13. O. Toirov, T. Kamalov, U. Mirkhonov, S. Urokov, D. Jumaeva, The mathematical model and a block diagram of a synchronous motor compressor unit with a system of automatic control of the excitation // E3S Web of Conferences, 288, 01083, (2021), https://doi.org/10.1051/e3sconf/202128801083
14. Taniev M., Mirkhonov U., Rakhmatova M., Isakov F. Study of The Substitution Scheme of The Parameters of a Phase-Rotor Induction Generator // January 2023 AIP Conference Proceedings 2552(1):060010 DOI:10.1063/5.0130746. 2021. Vol. 3. pp. 340–347.
15. O. Toirov, S. Urokov, U. Mirkhonov, H. Afrisal, D. Jumaeva, Experimental study of the control of operating modes of a plate feeder based on a frequency-controlled electric drive, // E3S Web of Conferences, SUSE-2021, 288, 01086 (2021). https://doi.org/10.1051/e3sconf/202128801086
16. D. Bystrov, S. Giyasov, M. Taniev, S. Urokov. NISS2020: Proceedings of the 3rd International Conference on Networking, Information Systems & Security, 49, p. 1–4 (2020), https://doi.org/10.1145/3386723.3387868.
17. S. Khalikov, Diagnostics of pumping units of pumping station of machine water lifting, // E3S Web of Conferences 365, 04013, (2023). https://doi.org/10.1051/e3sconf/202336504013
18. O. Toirov, I. Khujaev, J. Jumayev, M. Hamdamov, Modeling of vertical axis wind turbine using Ansys Fluent package program, // E3S Web of Conferences 401, 04040 (2023). https://doi.org/10.1051/e3sconf/202340104040
19. D. Bystrov, M. Gulzoda, Y. Dilfuza, Fuzzy Systems for Computational Linguistics and Natural Language (2020) // ACM International Conference Proceeding Series, https://doi.org/10.1145/3386723.3387873
20. O. Toirov, S. Abdi Yonis, Z. Yusupov, A. Habbal, Control Approach Of A Grid Connected Dfig Based Wind Turbine Using Mppt And Pi Controller, // Advances in Electrical and Electronic Engineering, 21, 3, (2023). https://doi.org/10.15598/aeee.v21i3.5149
21. D. Jumaeva, A. Abdurakhimov, Kh. Abdurakhimov, N. Rakhmatullaeva, O. Toirov, Energy of adsorption of an adsorbent in solving environmental problems, // E3S Web of Conferences, SUSE-2021, 288, 01082 (2021). https://doi.org/10.1051/e3sconf/202128801082
22. O. Toirov, M. Khalikova, D. Jumaeva, S. Kakharov, (2023) Development of a mathematical model of a frequency-controlled electromagnetic vibration motor taking into account the nonlinear dependences of the characteristics of the elements, // E3S Web of Conferences 401, 05089, (2023). https://doi.org/10.1051/e3sconf/202340105089
23. S. Khalikov. Analysis of the safety of pumping units of pumping stations of machine water lifting in the function of reliability indicators, // E3S Web of Conferences 365, 04010 (2023), https://doi.org/10.1051/e3sconf/202336504010
24. O. Toirov, D. Jumaeva, U. Mirkhonov, S. Urokov, S. Ergashev, Frequency-controlled asynchronous electric drives and their energy parameters, // AIP Conference Proceedings 2552, 040021, (2022). https://doi.org/10.1063/5.0218808
25. T. Sadullaev, D. Abdullaev, D. Jumaeva, Sh. Ergashev, I.B. Sapaev, Development of contactless switching devices for asynchronous machines in order to save energy and resources, // E3S Web of Conferences 383, 01029, (2023). https://doi.org/10.1051/e3sconf/202338301029
26. O. Toirov, S. Khalikov, Algorithm and Software Implementation of the Diagnostic System for the Technical Condition of Powerful Units, // E3S Web of Conferences 377, 01004, (2023). https://doi.org/10.1051/e3sconf/202337701004
27. D. Jumaeva, Z. Okhunjanov, U. Raximov, R. Akhrorova. Investigation of the adsorption of nonpolar adsorbate molecules on the illite surface, // Journal of Chemical Technology and Metallurgy, 58, 2, (2023). https://doi.org/10.59957/jctm.v58i2.61
28. O. Toirov, K. Alimkhodjaev, A. Pardaboev, Analysis and ways of reducing electricity losses in the electric power systems of industrial enterprises, // E3S Web of Conferences, SUSE-2021, 288, 01085 (2021). https://doi.org/10.1051/e3sconf/202128801085

29. M. Taniev, B. Safarov, Z. Toirov. Simulation model of an asynchronous generator integrated with a power supply system at different wind speeds AIP Conference Proceedings, 3331 (1), 060025, (2025). https://doi.org/10.1063/5.0305672